CHEMICAL ENGINEERING TRANSACTIONS
VOL. 50, 2016
A publication of AIDIC
The Italian Association of Chemical Engineering
Online at www.aidic.it/cet
Guest Editors: Katharina Kohse-Höinghaus, Eliseo Ranzi

ISBN 978-88-95608-41-9; **ISSN** 2283-9216
DOI: 10.3303/CET1650021

Experimental and Numerical Studies of Electric Field Effects on Biomass Thermo-chemical Conversion

Inesa Barmina[a], Antons Kolmickovs[a], Raimonds Valdmanis[a], Maija Zake[*a], Harijs Kalis[b]

[a]Instutute of Physics, University of Latvia, 32 Miera Street, Salaspils-1, LV-2169, Latvia
[b]Institute of Mathematics and Informatics, University of Latvia, 29 Raina boulevard, Riga, LV-1459, Latvia
mzfi@sal.lv

Experimental study and mathematical modelling were aimed to provide electric control of biomass thermo-chemical conversion and analysis of the DC electric and electromagnetic effects on combustion dynamics to obtain a cleaner and a more effective heat energy production. Mathematical modelling of the formation of flame velocity and temperature profiles was performed considering the Lorentz force effect on the flame. The results of numerical simulation show that increasing the electrodynamic Lorentz force parameter P_e leads to the increase of flame vorticity enhancing thus the fuel mixing with the air and to the correlating decrease of the flame temperature and reaction rates. Experimental study and analysis of the DC field effect on development of the swirling flow dynamics shows that the electric field-induced ionic wind disturbs the formation of the swirling flow velocity field by enhancing the upstream swirling flow formation and mixing of the axial flow of combustible volatiles with an upstream air swirl. The field-enhanced mixing of the axial flow of volatiles with an air leads to improvement of combustion conditions and to an increase in combustion efficiency giving a more complete combustion of volatiles by increasing the produced heat energy at thermo-chemical conversion of biomass.

1. Introduction

The use of swirl to stabilize flow dynamics and improve mixing (Gupta et al., 1984) in combustion systems is well known. The detailed study of swirling flow formation has shown that the flow structure and dynamics are highly influenced by the swirl intensity depending on the swirl number (S) of inlet flow. For strongly swirled non-premixed flames (S > 0.6), a central toroidal recirculation zone develops that promotes swirl enhanced mixing of the axial fuel flow with the air swirl and causes enhanced heating and combustion of the fuel components, but the flame flow instability increases. With the weak flame swirl (S < 0.6), a gradual mixing of the axial flow of volatiles with the surrounding air swirl forms a non-recirculating flow and causes cleaner and more complete fuel combustion with lower levels of harmful emission. The experimental study of the swirl effect on combustion dynamics at thermo-chemical conversion of biomass has shown that the development of flow velocity profiles is influenced by the upstream air swirl flow motion (Abricka et al., 2014). The upstream swirl formation enhances biomass thermal decomposition, mixing of the main reactants (the axial flow of volatiles with air) in a space below the air swirl inlet and improves the combustion conditions in the flame reaction zone.

An additional tool to improve and control the swirling flame stability, combustion efficiency and composition of products is the electric control of combustion dynamics. Theoretical analysis of the mechanism of the low voltage electric field and flame interaction allows the conclusion that the electrical body force $\vec{F} = en_{\pm}\vec{E}$ drives the positively and negatively charged gaseous species in the field direction (Lawton and Weinberg, 1969). This initiates the interrelated processes of heat and mass transfer (ionic wind effects), which could vary the flame temperature and composition providing cleaner heat energy production (Barmina et al., 2014; Zake et al., 2001). The present study is focused on the further development and analysis of the DC electrical and electromagnetic field effects on the swirling flame flow dynamics, which can be related to the ion wind (Lawton

Please cite this article as: Barmina I., Kolmickovs A., Valdmanis R., Zake M., Kalis H., 2016, Experimental and numerical studies of electric field effects on biomass thermo-chemical conversion, Chemical Engineering Transactions, 50, 121-126 DOI: 10.3303/CET1650021

and Weinberg, 1969) and Lorentz force effects (Shih-I, 1962) on the flame. More specific, the results of experimental study demonstrate the DC electric field-enhanced upstream air swirl motion with field-enhanced mixing of the flame components and more effective heat-energy production by minimizing the environmental impact of combustion systems. In addition, mathematical modelling and numerical simulation of the electromagnetic field effect on development combustion dynamics is used to illustrate and provide more detailed analysis of the Lorentz force effects on the formation of swirling flame structure and combustion conditions.

2. Experimental

The DC electric field effect on the processes developing downstream of the swirling flame flow at thermo-chemical conversion of biomass (wood) pellets is studied experimentally using a pilot-scale setup, which consists of two main parts: a biomass gasifier of inner diameter D (1), charged with biomass pellets of a total weight 240 g and a water-cooled combustor of length z (2) (Figure 1). Thermal decomposition of biomass pellets with an intensive release of combustible volatiles (CO, H2, CH4, C2H2, C2H4) is initiated using a propane flame flow (3) as an additional heat energy source. The primary axial (4) and secondary (5) swirling airflows are used to promote the biomass gasification and to provide the complete combustion of the volatiles downstream of the water-cooled combustor.

The electric field is applied to the bottom of the combustor using a single electrode configuration when the top of the axially inserted electrode (6) is located below the swirling air inlet nozzles (z/D ≈ -0.3). The bias voltage of the electrode (U) is positive relative to the grounded water-cooled walls of the pilot device. To restrict the formation of a corona discharge, the bias voltage of the axially inserted electrode is limited to U = 2.4 kV, while the ion current is limited to 2 mA. To measure the flame velocity profiles, a pitot tube and a Testo 435 flow meter were used. The flame temperature was measured using Pt/Pt-Rh thermocouples and a data PC-20TR data acquisition card (BMC Messsysteme GmbH). For spectral analysis of the products composition at biomass thermal decomposition, a FTIR spectrometer was used. For local measurements of the flame temperature and composition (i.e. the mass fraction of volatiles CO, H2), the volume fraction of the main product (CO2), and the combustion efficiency, a Testo 350 gas analyzer was used. Calorimetric measurements of the cooling water flow were made to estimate the electric field effect on the heat-energy production at different stages of biomass thermo-chemical conversion.

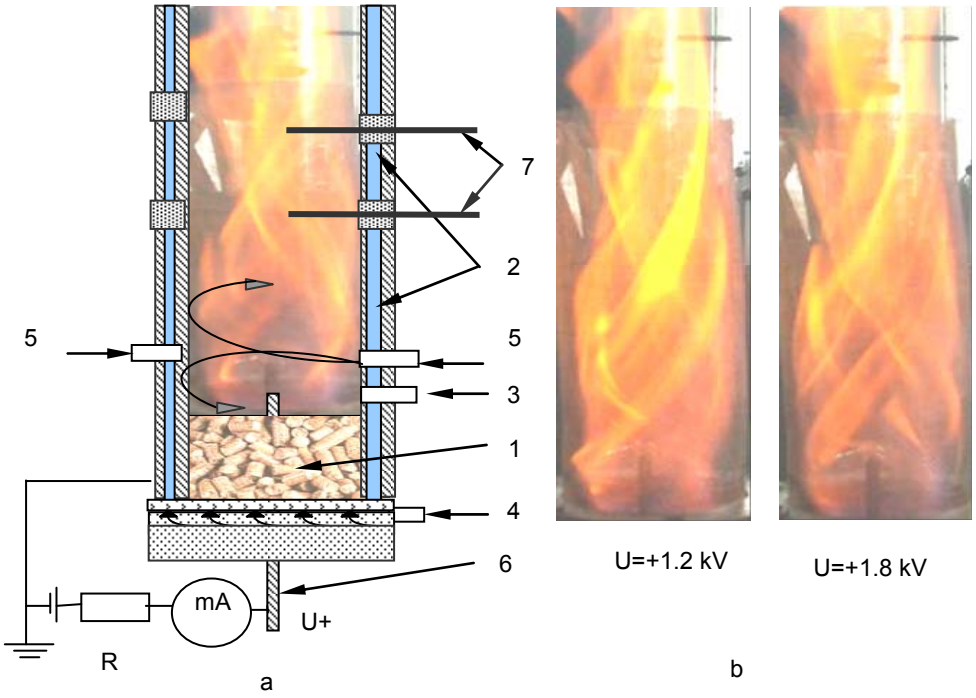

Figure 1: a) Schematic view of the small-scale pilot device: 1 – gasifier, 2 - combustor; 3 - propane flame inlet; 4 - primary air supply; 5 – secondary swirling air supply; 6 - axially inserted electrode; 7 - openings for diagnostic tools (a); the electric field effect on the flame structure (b).

3. Mathematical modelling

Mathematical modelling of the formation of swirling flame velocity and temperature profiles was made considering the effect of the electromagnetic force on the flame. The electromagnetic force is generated by an electric current I of density j_0 in a coil electrode surrounding the flame at the inlet of the cylindrical pipe (combustor). The electric current creates the radial B_r and axial B_z components of the induced magnetic field and generates the axial $F_z = -B_r j_0$ and radial $F_r = B_z j_0$ electromagnetic forces (Lorentz force) and the azimuthal component of the force curl $f = -j_0 B_r / r'$. The azimuthal component of the vector potential A_φ and the Biot-Savart law were used (Buikis et al., 2002) to investigate and calculate the distribution of the electromagnetic field components $B_r = -\partial A_\varphi / \partial z, B_z = \partial (r A_\varphi) / r \partial r$ for an axially symmetric system of the electric current: $r \in [r_0, R_0], z \in [z_1, z_2], \varphi \in [0, 2\pi]$:

$$A_\varphi(r,z) = \frac{\mu}{2\pi} \int_{r_0}^{R_0} \int_{0}^{2\pi} \int_{z_1}^{z_2} \frac{j_\varphi \xi \cos(\varphi)}{\sqrt{\xi^2 + r^2 - 2r\xi\cos(\varphi) + (z-\eta)^2}} d\xi\, d\varphi\, d\eta, \tag{1}$$

where $\mu = 4\pi 10^{-7}$ N/A^2 is the coefficient of magnetic permeability of the medium. For the coil electrode with radius ε ($R_o = r_0$, $z_1 = z_2 = 0$, j_φ = const):

$$B_r = \frac{\mu I}{2\pi} \frac{z}{c\, r} \left(\frac{z^2 + r_0^{\,2} + r^2}{z^2 + (r_0 - r)^2} E(k) - K(k) \right), \; B_z = \frac{\mu I}{2\pi} \frac{1}{c} \left(\frac{z^2 - r_0^{\,2} - r^2}{z^2 + (r_0 - r)^2} E(k) + K(k) \right), \tag{2}$$

where K (k), E (k) are the total elliptical integrals of the first and second kinds, $k = 2\sqrt{r_0 r} / c$, $c = \sqrt{(r_0 + r)^2 + z^2}$ and $I = j_\varphi \pi \varepsilon^2 = 120$ μA.

For numerical simulation of the stream function Ψ ($r\rho w = \partial \psi / \partial r, r\rho u = \partial \psi / \partial x$), the circulation $\tilde{v} = v\, r$ and modified vorticity $\tilde{\zeta} = \zeta / r$ with low Mach number (Choi et al., 2007) approximation, the following flow equations were used:

$$\begin{cases} \dfrac{\partial \tilde{\zeta}}{\partial t} + u \dfrac{\partial \tilde{\zeta}}{\partial r} + w \dfrac{\partial \tilde{\zeta}}{\partial x} + 0.5 \dfrac{T}{r} J\left(T^{-1}, V^2\right) = \dfrac{S^2 T}{r^4} \dfrac{\partial (T^{-1} \tilde{v}^2)}{\partial x} - P_e \dfrac{\tilde{B}_r}{r^2}, \\ \dfrac{\partial \psi}{\partial t} = \dfrac{\partial}{\partial x}\left(T \dfrac{\partial \psi}{\partial x} \right) + r \dfrac{\partial}{\partial r}\left(\dfrac{T}{r} \dfrac{\partial \psi}{\partial r} \right) + r^2 \zeta, \dfrac{\partial \tilde{v}}{\partial t} + u \dfrac{\partial \tilde{v}}{\partial r} + w \dfrac{\partial \tilde{v}}{\partial x} = 0, \end{cases} \tag{3}$$

where in the dimensionless form, all lengths are scaled to $r_0 = 0.05$ m ($x = z/r_0$), the velocities to $U_0 = 0.01$ m/s, and the temperature to $T_0 = 300$ K; $V = \sqrt{u^2 + w^2}$; $\tilde{B}_r = \dfrac{B_r}{B_0}$; $B_0 = \dfrac{\mu I}{2\pi r_0} = 0.410^{-5} I[T]$; $J(a,b) = \dfrac{\partial a}{\partial x}\dfrac{\partial b}{\partial r} - \dfrac{\partial a}{\partial r}\dfrac{\partial b}{\partial x}$ is the Jacobian; $\zeta = \dfrac{\partial u}{\partial x} - \dfrac{\partial w}{\partial r}$; $P_e = \dfrac{B_0 j_0 r_0}{\rho_0 U_0^2}$ is the electrodynamics' force parameter and $S = V_0/U_0$ is the swirl number. The equation (3) is transformed to non-steady conditions.

A 2-D reaction-diffusion system of the non-linear differential equations was used to analyze the effect of the

$$\begin{cases} \dfrac{\partial T}{\partial t} + u \dfrac{\partial T}{\partial r} + w \dfrac{\partial T}{\partial x} = \dfrac{L_e}{\rho Pe} \Delta T + \beta A C \exp\left(-\dfrac{\delta}{T} \right), \\ \dfrac{\partial C}{\partial t} + u \dfrac{\partial C}{\partial r} + w \dfrac{\partial C}{\partial x} = \dfrac{1}{\rho Pe} \Delta C - A C \exp\left(-\dfrac{\delta}{T} \right), \end{cases} \tag{4}$$

induced forces on the formation of temperature and concentration profiles:

where pT = 1; $Pe = \rho_0 U_0 r_0 / D$ = 10; $Le = \lambda / c_p D$ = 1 are the Peclet and Lewis numbers; $\beta = B / c_p T_0$ = 5 is the heat-release parameter; $\tilde{A} = Ar_0 / U_0$ = 5000 is the scaled pre-exponential factor; $\delta = E / RT_0$ = 10 is the scaled activation energy; Δ is the Laplace operator; $D = 5 \cdot 10^{-5}$ m^2/s is the molecular diffusivity; $\lambda = 5 \cdot 10^{-2}$ J/s·m·K is the thermal conductivity; c_p = 1000 J/kg·K is the specific heat at constant pressure; $B = 1.5 \cdot 10^6$ J/kg; $A = 10^4$ 1/s, $E = 2.5 \cdot 10^4$ J/mol are the specific heat release, the reaction-rate pre-exponential factor, and the activation energy; R = 8.314 J/mol·K is the universal gas constant.

4. Results and discussion

4.1 Results of numerical simulation

For numerical simulation the boundary conditions (BCs) are the following:

1) along the flow axis r = 0 - $\tilde{v} = 0$, $\psi = 0$ $\partial T / \partial r = \partial C / \partial r = \partial \tilde{\zeta} / \partial r = 0$ (the symmetry conditions),

2) at the wall r = 1 - $\tilde{v} = 0$, $\psi = q$, $\zeta = 0$, $\partial T / \partial r = \partial C / \partial r = 0$, $\partial T / \partial r + Bi(T - 1) = 0$,

3) at the pipe outlet x = x_0 - $u = 0$, $\partial T / \partial x = \partial C / \partial x = \partial \tilde{\zeta} / \partial x = \partial \tilde{v} / \partial x = \partial \psi / \partial x = 0$,

At the pipe inlet boundary conditions are: $u = 0$, $T = 1$; for $r \in [0,1]$ and $w = 1$, $C = 1$, $\psi = 0.5 r^2$, $\tilde{v} = 0$, $\tilde{\zeta} = 0$ for $r \in [0, r_1]$.

Here $Bi = hr_0 / \lambda$ = 0.1 is the Biot number, and $q = 0.5 r_1^2$ is the dimensionless fluid volume. The applied approach seeks the steady solution as the time asymptotic limit of the solutions of the unsteady equations. The distributions of the stream function, azimuthal component of velocity, flow vorticity and temperature were calculated using the implicit FDS with the upwind differences in the space, the ADI method, and under relaxation.

The results of the numerical simulation show that the increase of the electrodynamic force parameter P_e (Lorentz force) leads to variation of the flow stream function with the increase of flame vorticity along the outside part of the reaction zone (r/r_0) > 0.5 (Figure 2) and maximal flow velocity by enhancing the fuel mixing with the air and decreasing the flame temperature and reaction rate (Table 1).

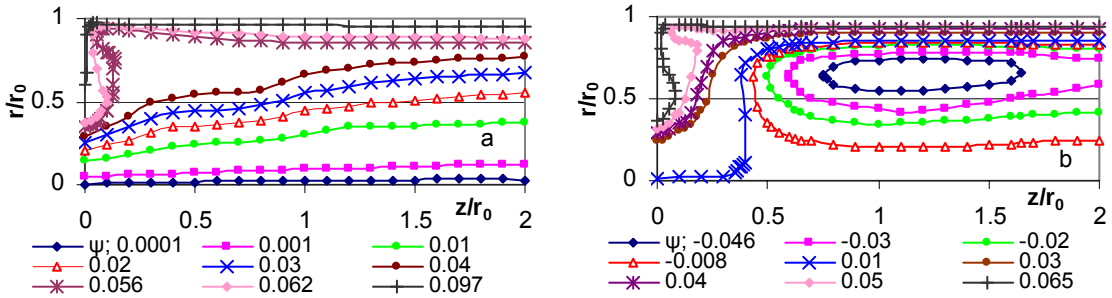

Figure 2: The flow stream function for P_e = 0, S = 1 (a) and for P_e = 1, S = 1 (b).

Table 1: The values of P_e, S, T_{av}, maxU, maxR, maxT, max|ζ|, min Ψ, for x_0=2

P_e	S	T_{av}	maxU	maxR	maxT	max|ζ|	min Ψ
0.0	1	3.000	5.402	805.97	5.877	137.61	0
0.5	1	2.883	5.463	805.29	5.873	139.85	-0.0056
1.0	1	2.759	5.545	804.97	5.861	143.38	-0.0460

4.2 Results of experimental study

If the DC electric field is applied to the flame base, the formation of the flow dynamics and swirl intensity are influenced by the field-induced ionic wind effect, which enhances the radial and reverse axial mass transfer of the flame species in a field direction (Figure 3-a-d). As follows from Figure 3-a, the field-enhanced reverse axial mass transfer and upstream air swirl motion results in an increase in swirl number with the correlating decrease in axial flow velocity (Figure 3-b) at the primary stage of swirling flow formation (z/D ≈ 0.7).

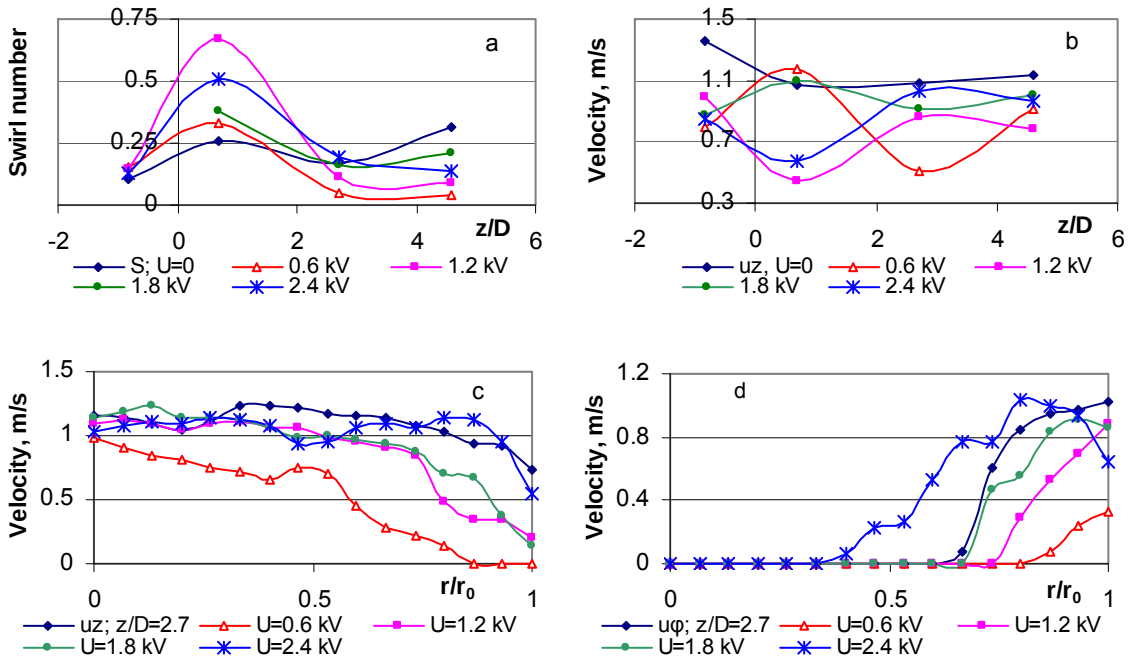

Figure 3: The electric field effect on the axial distribution of the flow swirl number (a), average values of the axial flow velocity (b), the radial profiles of axial (c) and azimuthal (d) flow velocity components.

The strongest deformation of the flow velocity profiles is at relatively low bias voltages (U < 1.2 kV), when the occurrence of the peak value of the swirl number at the flame base is detected (Figure 3-a). It should be noted that the field-induced variation of the axial velocity (Figure 3-b) indicates the development of flow instability. The development of flow instability was confirmed by the field-enhanced formation of a double-helical structure of the swirling flow field (Figure 1-b) and can be related to a pre-breakdown stage of swirling flow (Billant et al., 1998). A reasonable explanation of the field-enhanced formation of the pre-breakdown stage is the field-enhanced increase of the swirl number at the flame base up to the critical value (S ≈ 0.66) (Gupta et al, 1984). The axial flow velocity profiles and flow dynamics was observed to stabilize at z/D > 2.

Once the field-enhanced upstream swirl motion occurs, the absorbance of the volatiles (CO, C_2H_2) increases by about 15-18 % at the primary stage of the flame formation (z/D = 0.7) (Figure 4-a) evidencing that the field–enhanced reverse air swirl motion close to the surface of a biomass layer results in the field-enhanced thermal decomposition of biomass. This was confirmed by an increase of the biomass weight loss rate by about 12 %. The results of the previous investigations show (Abricka et al., 2014) that the upstream swirl flow reversing from the biomass layer enhances the convective transport of the volatiles along the flow axis. This leads to the formation of a sharp peak of the mass fraction of volatiles (CO, H_2) close to the flow axis (Figure 4-c). The maximum value of the mass fraction of volatiles at the flow axis is attributed to the bias voltage of the axially inserted electrode U = 1.2 kV and corresponds to the formation of the peak value of swirl intensity at the flame base (Figure 3-a). In addition to the field-enhanced biomass thermal decomposition, the field enhanced swirl motion close above the biomass layer results in a enhanced mixing of the axial flow of the volatiles with the air improving the volatiles combustion conditions in the flame reaction zone (z/D = 2.7). This leads to a decrease of the CO and H_2 peak mass fraction in the products (Figure 4-b) with the correlating increase of the average volume fraction of CO_2 from 9.5 to 10.8 % (Figure 4-d), the flame temperature near the flow axis, the average value of the combustion efficiency by about 4.5 % and of the produced heat energy by about 8-10 % determining cleaner heat energy production with the radial expansion of the reaction zone. The reverse field effect on the combustion of volatiles was observed at the field-enhanced increase of the axial flow velocity for U>1,2kV, when the CO_2 volume fraction in the flame reaction zone decreased (Figure 3-d). This finding suggests that the shape of the flame composition profiles is affected by the field-induced variations of the residence time of reactions (t_r), which increases when the average and local values of the axial flow velocity ($u_r \approx 1/t_r$) decrease, providing more complete combustion of volatiles further downstream (z/D > 2.7) where a 2-3 % increase of the CO_2 volume fraction, combustion efficiency, and produced heat energy was observed for U = 2.4 kV and I = 1.75 mA.

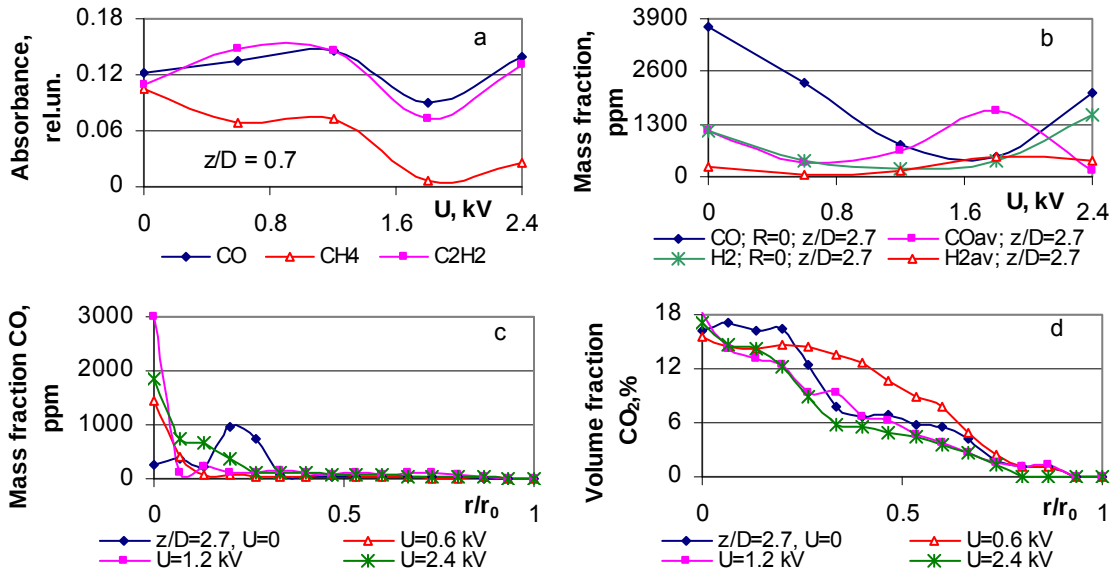

Figure 4: The electric field effect on the absorbance of volatiles at the bottom of the combustor (a), on the mass fraction of volatiles in the flame reaction zone (b) and on the flame composition profiles (c, d).

5. Conclusions

The mathematical modelling of the combustion control using the electromagnetic Lorentz force effect on the formation of velocity profiles and flame reaction zone has proved that the increase of the electrodynamic force parameter P_e increases the maximal velocity, strengthening the flow vorticity and assuring the field-enhanced mixing of the fuel flow with the air with a decrease of the temperature and reaction rate maximum values.
Experimental study of the electric field effect on the development of flow velocity fields, flow structure and composition was carried out to ascertain the DC electric field effect on the combustion dynamics at thermo-chemical conversion of biomass, which can be related to the field-induced ionic wind effect. The results of experimental study allows the conclusion that the DC field-enhanced reverse upstream swirl motion leads to enhanced biomass thermal decomposition with the enhanced formation of the volatiles. Moreover, the field-enhanced swirl motion leads to enhanced mixing of the axial flow of volatiles with the air at the bottom of the combustor, resulting in enhanced combustion of the volatiles with an increase of the combustion efficiency and produced heat energy, determining cleaner and more effective heat energy production.

Acknowledgments

The authors would like to acknowledge the financial support of the Latvian research grant No. 2014/623.

Reference

Abricka M., Barmina I., Valdmanis R., Zake M., 2014, Experimental and numerical study of swirling flows and flame dynamics, Latvian Journal of Physics and Technical Sciences, 51, N4, 25-40.
Barmina I., Zake M., Valdmanis R., 2014, Electric field-induced variations of combustion dynamics, Chemical Engineering Transactions, 39, 1531-1536, DOI: 10.3303/CET1439256
Billant P., Chomaz J.M., Huerre P., 1998, Experimental study of vortex breakdown in swirling jets, J. Fluid Mech., 376, 183-219.
Buikis A., Kalis H., 2002, Numerical modelling of heat and magnetohydrodynamic flows in finite cylinder, Computational methods in applied mathematics, 2, N3, 243-259.
Choi J.J., Rusak Z., Kapila A.K., 2007, Numerical simulation of premixed chemical reactions with swirl. Combustion theory and modelling, 6, 11, 863-887.
Gupta A.K., Lilley D.G., Syred N., 1984, Swirl Flows, Abacus Press, UK, 588.
Lawton J., Weinberg F., 1969, Electric Aspects of Combustion. Clarendon Press, Oxford, England, 650.
Pai S.I., 1962, Magnetogasdynamics and plasma dynamics, Springer-Verlag, 302.
Zake M., Barmina I., Turlajs D., 2001, Electric field control of polluting emissions from a propane flame, GLOBAL NEST: the International Journal, 3, N2, 95-111.